Published in "Optica 4(3): 361–366, 2017"
which should be cited to refer to this work.

Photonic hyperuniform networks obtained by silicon double inversion of polymer templates

Nicolas Muller,[1] Jakub Haberko,[2] Catherine Marichy,[1,3] and Frank Scheffold[1,*]

[1]Department of Physics, University of Fribourg, CH-1700 Fribourg, Switzerland
[2]Faculty of Physics and Applied Computer Science, AGH University of Science and Technology, al. Mickiewicza 30, 30-059 Krakow, Poland
[3]Université de Lyon, Laboratoire des Multimatériaux et Interfaces, Villeurbanne Cedex, 69622 Lyon, France
*Corresponding author: Frank.Scheffold@unifr.ch

Hyperuniform disordered networks belong to a peculiar class of structured materials predicted to display isotropic complete photonic bandgaps for a refractive index contrast larger than 3. The practical realization of such photonic designer materials is challenging, however, as it requires control over a multi-step fabrication process on optical length scales. Here we report the direct-laser writing of three-dimensional hyperuniform polymeric templates followed by a silicon double inversion procedure leading to high-quality network structures made of polycrystalline silicon. We observe a pronounced gap in the shortwave infrared centered at a wavelength of $\lambda_{Gap} \simeq 2.5$ μm, in good agreement with numerical simulations. In the experiments the typical structural length scale can be varied between 2 and 1.54 μm, leading to a blueshift of the gap accompanied by an increase of the silicon filling fraction.

OCIS codes: (160.3918) Metamaterials; (160.5293) Photonic bandgap materials; (160.5298) Photonic crystals; (290.7050) Turbid media.

1. INTRODUCTION

Photonic crystal structures have drawn a lot of attention over the past decades due to their potential applications in optical circuits and photon guiding [1], improved laser sources [2], negative refractive index material properties [3], or tunable optical devices [4,5]. However, the routine design of full bandgap materials in three dimensions for optical wavelengths has proven elusive [3,6–10]. Recently, disordered and isotropic photonic materials have been suggested as an alternative [11–17]. A hyperuniform structure combined with short range order and an open network architecture is widely considered to be a strong candidate for an optimized photonic material design [13,14,18]. The isotropic structure should offer advantages such as the possibility to incorporate waveguides with arbitrary bending angles [1,19,20]. Numerical calculations in two and three dimensions suggest the presence of a full photonic bandgap in the near-infrared if the material is made out of a material with an refractive index $n > 3$ in air, such as silicon [13,14]. Previous experimental studies of hyperuniform photonic materials have reported partial and full bandgaps for 2D hyperuniform network structures in the microwave regime [19,21]. Recently we demonstrated the fabrication of high refractive index three-dimensional (3D) hyperuniform materials by coating polymer templates with TiO_2 and silicon [16]. The final materials contained some titania (TiO_2, $n \simeq 2.4$), lowering the refractive index contrast slightly. The gold standard to achieve silicon photonic bandgap materials is the silicon double-inversion method, a rather complex multi-step process to transfer polymer templates into silicon replica [22,23]. Despite its complexity, it has been successfully applied to periodic structures [23–25]. Full photonic bandgaps have been reported for silicon woodpile photonic crystals in the shortwave infrared [23] and the near-infrared at telecom wavelengths [26]. The application of this approach to open hyperuniform network structures is even more difficult. In particular, retaining the mechanical stability of the network is a challenging task considering the harsh conditions when removing the sacrificial material components after each processing step. Here we report the successful realization of a silicon double-inversion approach applied to hyperuniform network structures designed by direct-laser writing (DLW) into a polymer photoresist [23,25,27].

2. FABRICATION

We first fabricate polymeric templates of height $h = 5.5$ μm and a footprint of approximately 65 μm × 65 μm with DLW into a liquid negative-tone photoresist as reported previously in [28,29]. As a seed pattern, we use the center positions of a jammed assembly of spheres [30], which is then numerically converted into a 3D hyperuniform (HU) network structure by following the procedure described in Ref. [28]. The average distance between the points is set by the diameter of the jammed spheres and is denoted by a. It sets the intrinsic length scale of the structure similar to the lattice constant of a photonic crystal. Consequently, a determines the wavelength of the observed photonic features. The design protocol consists of mapping the seed

pattern into tetrahedrons by performing a Delaunay tessellation. Then, the centers of mass of the tetrahedrons are connected, resulting in a tetravalent network structure of interconnected rods with the desired structural properties. The volume filling fraction ϕ and the mean rod diameter $\langle D \rangle$ are linked by $\phi \approx 3.5(\langle D \rangle / a)^2$ for $\phi < 0.4$ [16]. In the fabrication process, the rods acquire an ellipsoidal cross section, and an effective value of $\langle D \rangle$ can be calculated by taking the square root of the product between the two axes of the ellipse. In the present work, the characteristic structural length scale a is varied over a range $a = 1.54$–2 μm. The resulting polymer templates are therefore very open structures with a volume filling fraction of only about 15% for a mean rod diameter of $\langle D \rangle \simeq 350$ nm [28,29], Fig. 1(a). Next, these polymer structures are completely infiltrated with zinc oxide using atomic layer deposition (ALD) at a temperature of 110°C, low enough to preserve the integrity of the template. The sample is exposed to an Ar plasma to remove the excess of ZnO that forms on top of the structure. Then the polymer–ZnO composite material is heated to a temperature of 500°C for >5 h to thermally degrade the polymer. The ZnO inverse structure is infiltrated with amorphous silicon using chemical vapor deposition (CVD) at 480°C [1,25]. To obtain the positive replica, the ZnO is removed by wet etching with aqueous hydrochloric acid. At this stage, the photonic features in the optical spectrum are masked by the pronounced scattering from the Si overlayer (Fig. S3 in Supplement 1). Further tempering of the structure at 600°C for >8 h transforms the as-deposited amorphous silicon into its brittler polycrystalline phase ($n(\lambda = 2.5\ \mu\text{m}) \simeq 3.44$) [31]. Subsequent Ar-$SF_6$ plasma etching reduces the thickness of the Si overlayer up to a point at which it starts to break off. When doing so, the bare network structure becomes accessible [Fig. 1(b)].

A. Direct Laser Writing

Polymeric templates on the mesoscale are fabricated using a commercially available DLW system (Photonic Professional GT, Nanoscribe GmbH, Germany) in dip-In configuration. [28,29] The digitally designed structures with a height of 6 μm are written on infrared transparent CaF_2 substrates (Crystan, UK) by dipping an oil-immersion objective (63× , NA = 1.4) inside a liquid negative-tone photoresist (IP-DIP, Nanoscribe GmbH, Germany). The writing process is started in a virtual depth of approximately 0.5 μm inside the glass substrate, and thus the nominal height is 5.5 μm. The latter is needed to guarantee a continuous laser writing process along the axial direction, which is necessary to ensure the adhesion of the polymer template to the substrate. Moreover, the actual height of the sample is further reduced by 10%–20% due to polymer shrinkage in the development process and the subsequent etching steps. We thus estimate the actual height to be $h = 4.75 \pm 0.5$ μm. Massive square walls are written around each structure to improve the mechanical stability during the development procedure and the post-processing. The photopolymerized samples are developed in two successive baths of propylene glycol monomethyl ether acetate (PGMEA) for twice 10 min and consecutively rinsed in a bath of isopropanol for 8 min. Gentle drying is ensured by redirecting a stream of N_2 through a bubbler filled with isopropanol onto the sample.

B. Silicon Double Inversion

The DLW-produced polymeric HU structures are infiltrated with ZnO using ALD. The deposition is carried out in a commercial ALD reactor (Savannah 100, Cambridge Nanotech, Inc.) operating in exposure mode at a moderate temperature of 110°C. Slow heating and cooling ramps are set to prevent thermal degradation

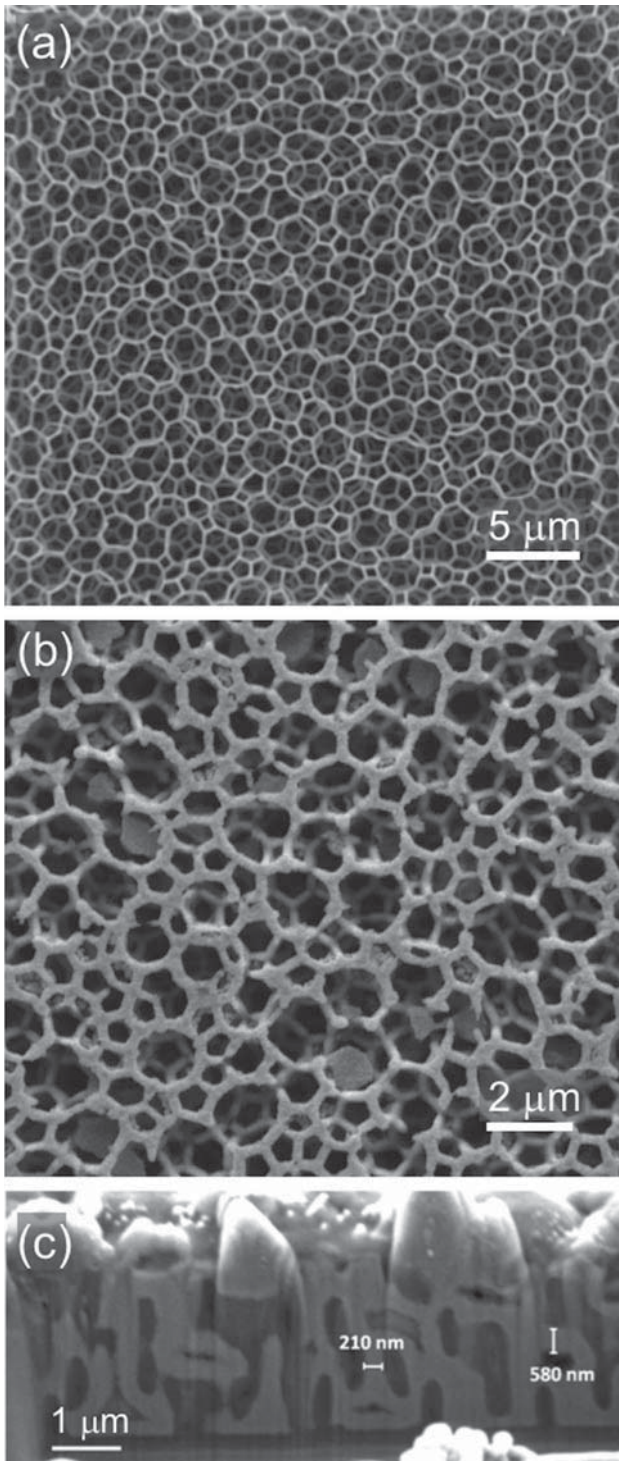

Fig. 1. SEM of hyperuniform disordered network structures. (a) Top view of a polymer template with $a = 2$ μm and height $h = 5.5$ μm. (b) Image of the back side of an $a = 1.82$ μm and $h = 5.5$ μm structure composed of polycrystalline silicon acquired after the silicon double-inversion process. The image confirms that the structure was completely infiltrated during the procedure. (c) Close-up view of a FIB cross section of a Si–ZnO composite structure reveals the bulk network structure of solid silicon rods. The dimensions of the rods in-plane are determined to be approximately 210 nm × 580 nm, resulting in a silicon volume filling fraction of $\phi \approx 0.13$.

of the polymer structure. Diethylzinc (Strem Chemicals, Inc., >95% purity) and deionized (Milli-*Q*) water were chosen as metal and oxygen sources, respectively. Both precursors are kept in stainless steel reservoirs at room temperature and subsequently introduced by pneumatic valves under a carrier gas flow of 5 sccm N_2 (sccm denotes cubic centimeters per minute at standard temperature and pressure) into the reactor chamber. For the depositions, pulse durations of 0.015 s are chosen for both the metal precursor and the oxygen source. Each pulse is followed by a dwelling time of 5 s without N_2 flow and a purge of 60 s under 20 sccm N_2. With these parameters the nominal growth rate is 1.2 Å per cycle. Three-thousand ALD cycles are applied on the HU structures to guarantee complete infiltration. After the ALD process, the ZnO overlayer is removed by plasma etching (PE-100 Series, Plasma Etch, Inc.) with 20 sccm of Ar at a pressure of 0.4 torr (1 torr ≈ 133.3 Pa) and a power of 200 W. The etch rate is approximately 1.3 nm min^{-1}. Next, the polymeric fraction of the ZnO-photoresist composite structure is removed via calcination at 500°C for >5 h in a tube furnace [Gero, Type SR(A)]. Heating and cooling ramps of 100°C h^{-1} are chosen to avoid thermal deterioration and delamination of the structures. The ZnO inverse structures are subsequently infiltrated with amorphous silicon at 480°C by thermal CVD. The process is carried out in a custom built reactor operating at a base pressure of 9 Torr by slowly heating the structures with plateaus at 150°C, 250°C, 350°C, and 480°C and with a dwelling time between 15 and 30 min. This allows the structures to thermally stabilize. Disilane gas (Si_2H_6) (Linde, ≥ 99.998%) is used as precursor. The disilane flow is set to 2 sccm, yielding a growth rate of about 4.6 nm min^{-1}. The flow is maintained for 35 min at a pressure of 17 torr to completely infiltrate the network structures. The silicon overlayer is partially removed by employing plasma etching with a gas mixture of 10 sccm of Ar and 3 sccm of sulfur hexafluoride (SF_6) at a pressure of 0.3 torr and a power of 40 W. The etching rate is 25–30 nm min^{-1}. The remaining ZnO is then wet etched by applying a few drops of aqueous hydrochloric acid (10 vol. %) on the sample. After 1 min the sample is rinsed with DI water and the procedure is repeated three times until no zinc oxide remains. The sample is dried in a gentle flow of N_2. Next, the as-fabricated structures are tempered at 600°C for >8 h to transform the amorphous silicon into its polycrystalline phase. This procedure reduces the refractive index somewhat [10] but has also been suggested to lead to a lower residual absorption coefficient [26]. Consecutive plasma etching results in a further reduction of the silicon overlayer until it was observed to break off revealing the bare network structure.

C. Electron Microscopy

The structures are analyzed by scanning electron microscopy (SEM) (Sirion FEG-XL30 S, FEI) between 5 and 10 kV. The complete silicon infiltration is confirmed by analyzing cross sections of a focused ion beam (FIB) cut, as well as by the presence of solid Si rods on the back side of a structure that detached and flipped over during the inversion process. The FIB cuts reveal that the silicon rods possess an elliptical cross section oriented in plane [29] with lengths of about 210 and 580 nm along the short and long axes, respectively [Fig. 1(c)]. These values correspond to a mean rod diameter of $\langle D \rangle \approx \sqrt{210 \cdot 580}$ nm = 350 nm and a corresponding silicon volume fraction of $\phi \approx 0.13$ for $a = 1.82$ μm. The compositional analysis of the final structure by Energy Dispersive Spectroscopy (Fig. S4 and Table S1 in Supplement 1) indicates the presence of pure silicon.

D. Optical Characterization

The optical spectra of the hyperuniform disordered structures are recorded using a Fourier transform infrared spectrometer (Bruker Vertex 70, germanium-coated KBr beam splitter) connected to a microscope (Bruker Hyperion 2000, SiC globar light source, liquid N_2-cooled InSb detector) [Fig. 2]. The employed objective is a 36× Cassegrain with a numerical aperture of 0.52. Transmittance and reflectance of light incident under a cone of light between 10° and 30° relative to the surface normal are measured. Additional transmittance measurements with a reduced angular spread are performed by tilting the sample with

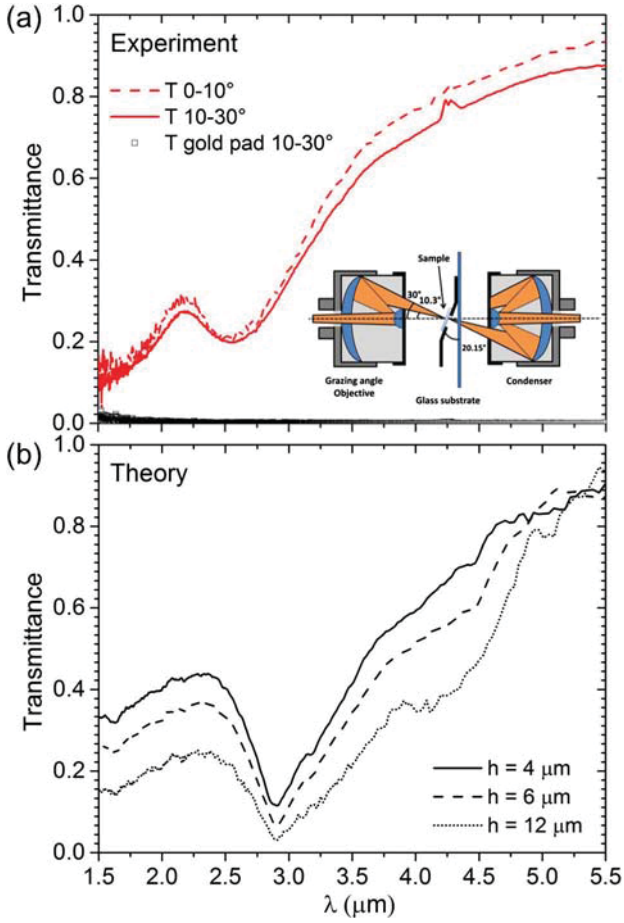

Fig. 2. (a) Fourier transform infrared spectroscopy (FTIR) of silicon hyperuniform network structures. Transmittance and reflectance spectra for a hyperuniform structure of $a = 1.82$ μm and height $h = 5.5$ μm recorded using a pair of Cassegrain objectives. The probing cone of light possesses an angular spread of 10°–30° with respect to normal incidence. Additional transmittance measurements are performed with an angular spread of 0°–10° with respect to the surface normal. Inset: FTIR spectrometer microscope sample chamber with Cassegrain objectives for illumination and detection of the transmitted and reflected light intensity. The tilted sample holder shown allows probing illumination under 0°–10° with respect to normal incidence when shadowing part of the Cassegrain objectives. Symbols: transmittance background level obtained from the measurement on a opaque gold pad. (b) FDTD simulations. The lines show the results obtained for a filling fraction of $\phi = 13\%$, $a = 1.82$ μm, $n = 3.4$, and for different heights h.

an appropriate holder and shadowing part of the Cassegrain objective such that a probing illumination under 0°–10° with respect to normal incidence is achieved [Fig. 2(a)] [26]. All spectra are normalized by a reference taken in air and on a gold pad for transmittance and reflectance measurements, respectively.

3. NUMERICAL SIMULATIONS OF LIGHT TRANSPORT

We perform 3D finite-difference time-domain (FDTD) simulations on hyperuniform silicon networks using the free software package MEEP (v.1.2) [32]. The simulations provide the total transmittance (T) and reflectance (R) ($T + R = 1$) as functions of frequency or wavelength. The hyperuniform dielectric networks are analyzed with a spatial discretization of 50 nm (Fig. S5 in Supplement 1). We take the elliptical cross section of the rods into account with an aspect ratio of 2.8, and the mean rod diameter is varied to simulate different filling fractions. The size of the simulated structure is chosen as $12a \times 12a \times 3a$. Periodic boundary conditions are applied along the x and y axes. Left and right of the sample, along the wave propagation direction z, we place perfectly matched layer (PML) absorbers (Fig. S5 in Supplement 1). Moreover, we add a region of free space between the PMLs and the structure to allow any probable evanescent fields to decay before reaching the PML region. The thickness of the PML is set to 7 μm and we have verified that this choice effectively suppresses back reflections for wavelengths $\lambda \leq 7$ μm.

4. DISCUSSION

The structural and chemical characterization shows that the double inversion of the hyperuniform network structures into silicon has been successful. Moreover, we observe a pronounced gap in transmittance at a central wavelength of $\lambda_{\mathrm{Gap}} \sim 2.5$ μm for a structure of height $h = 5.5$ μm and $a = 1.54$–2 μm, as shown in Figs. 2 and 3. The central position λ_{Gap} of the gap nor its width changes when measuring at oblique or normal incidence [Fig. 2(a)]. This is an important observation since disordered materials are structurally isotropic, and, therefore, the photonic features are expected to be nearly angularly independent [13]. The gap extends from $\lambda \approx 2.2$–3 μm [Fig. 3(a)] while at the same time no specular reflections are observed for the corresponding wavelengths, as shown in Fig. 3(b). While a reflection peak is a characteristic feature of photonic crystals, it is notably absent here [8,9,26,33]. This means that the reflected light is diffusely distributed over the whole hemisphere. Residual oscillations in some of the reflectance spectra can be attributed to Fabry–Perot interference effects.

As shown in Fig. 2(b), we find good overall agreement between the experiment and the FDTD simulations for a refractive index of $n = 3.44$ and a height of 4–5 μm. Numerical calculations of the density of states of equivalent hyperuniform disordered network structures have shown that a complete photonic bandgap appears for filling fractions of $\phi = 0.15$ - 0.4 and for refractive indices $n \geq 3$ [14]. The optimal filling fraction is predicted to be in the range $\phi = 0.15$–0.25. Indeed, it is in this region that we observe experimentally and numerically the most pronounced gaps.

To study different silicon filling fractions, we vary the typical structural length scale from $a = 2$ μm down to $a = 1.54$ μm (Fig. 3). Correspondingly, the central gap wavelength shifts from $\lambda_{\mathrm{Gap}} \approx 2.7$ μm to $\lambda_{\mathrm{Gap}} \approx 2.3$ μm. The cross section of the

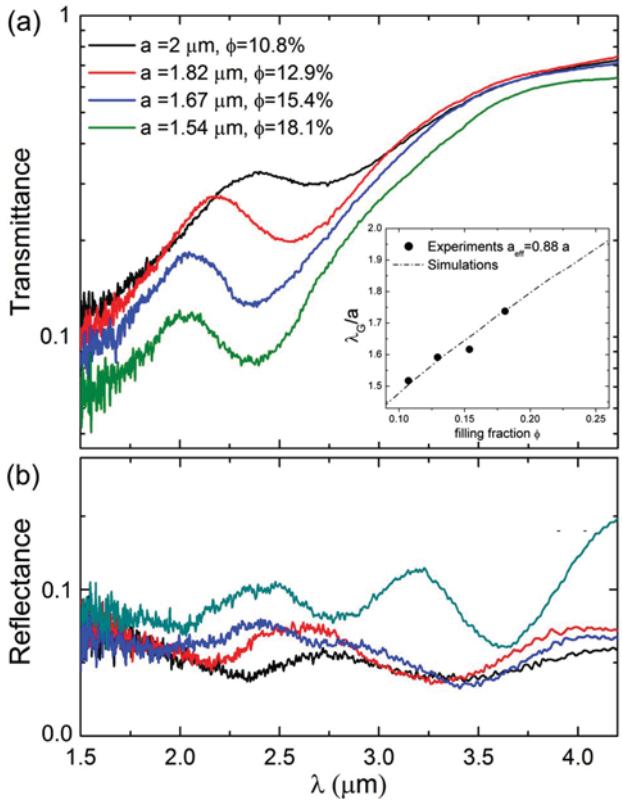

Fig. 3. (a) Transmittance and (b) reflectance spectra for $h \simeq 5.5$ μm and for different values of a. The data reveals a blueshift of the gap wavelength λ_G upon reducing the typical structure length scale of the seed pattern $a = 2$, at 1.82, 1.67, and 1.54 μm. Inset: dependence of the reduced gap wavelength λ_G/a on the silicon filling fraction. Solid circles: experiment results with $a_{\mathrm{eff}} = 0.88a$. Dashed–dotted line: FDTD simulations.

ellipsoidal rods remains unchanged as it is set by the DLW "pen." This means that, by continuously reducing the parameter a, the filling fraction increases from $\phi = 0.11$ to 0.18. The increased filling fraction leads to an effectively increased background refractive index that partially counteracts the blueshift of $\lambda_{\mathrm{Gap}}(a)$ when reducing a. With FDTD simulations we can study a larger range of filling fractions $\phi = 0.08$–0.26. As shown in the inset of Fig. 3(a), we again observe a shift of the reduced gap wavelength λ_{Gap}/a due to the increased effective (background) refractive index. The numerical simulations are in quantitative agreement with the experimental data if we assume $a_{\mathrm{eff}} \simeq 0.88a$. The slight mismatch can be explained by shrinkage of the network material during development of the polymer templates and the double-inversion procedure [34].

The onset of the pseudo-gap observed in the FDTD simulations appears to be more abrupt in comparison to the experimental data. To verify possible reasons for this discrepancy, we first performed FDTD calculations for a smaller rod refractive index ($n = 3.1$, Fig. S6 in Supplement 1). As expected, this leads to a weaker gap; however, the overall shape of the spectra remains essentially unchanged. Moreover, the chemical analysis indicates pure silicon, electron microscopy and FIB etching do not indicate that the rods are porous, and we therefore believe the rods consist of pure silicon with $n \simeq 3.4$ for the wavelengths probed. Also, the position of the gap predicted by FDTD matches the experimental

data well. We thus attribute the difference between the experimental and the numerical results to distortions in the structure, which lead to a smearing of the gap. Such distortions can be associated to uneven shrinkage and other imperfections, such as surface roughness, notable in Fig. 1(b), not taken into account in the numerical simulations.

For smaller wavelengths $\lambda \leq \lambda_{\mathrm{Gap}}$, the simulations and the experimental data deviate substantially. This is partially because, in the simulations, we calculate the total transmittance, whereas in the experiment, only light in a small cone is recorded. Moreover, the rough surface of the rods and other imperfections can lead to increased scattering in this regime. Similar deviations for $T(\lambda \leq \lambda_{\mathrm{Gap}})$ are commonly observed in periodic photonic structures, as well [26,33].

5. SUMMARY AND CONCLUSION

In this work, we have demonstrated the feasibility of fabricating 3D hyperuniform silicon networks by double inversion, and we have shown that the optical properties of the materials match those obtained from numerical simulations. This suggests that macroscopic, three dimensional hyperuniform photonic materials with a full bandgap can be realized if the structures are engineered on larger length scales, while at the same time conserving the structural integrity. In future work it would be desirable to reduce the structural length scales even further to bring the photonic bandgap closer to telecommunication wavelengths. As we have shown here, this can be realized by only reducing the cross section of the laser writing pen. Otherwise, the silicon filling fraction will increase beyond $\phi = 0.3$ and the photonic properties are expected to weaken [14]. Indeed, the necessary higher resolution can be achieved, for example, by employing a DLW scheme based on a 405 nm wavelength diode laser for the fabrication of polymeric templates as reported in [35] or by stimulated emission depletion inspired direct laser writing [27]. We believe the structural length scale a could then be reduced to below $a = 1$ μm, thereby opening the path toward a full isotropic bandgap at near-infrared wavelengths around $\lambda_{\mathrm{Gap}} \approx 1.3$–$1.5$ μm.

Funding. Adolphe Merkle Foundation; Fonds National de la Recherche Luxembourg (FNR) (3093332); Schweizerischer Nationalfonds zur Förderung der Wissenschaftlichen Forschung (SNF) (149867, 169074, NCCR Bio-Inspired Materials).

Acknowledgment. The authors thank Bodo Wilts for technical support and discussions. JH acknowledges the use of the TeraACMIN cluster at the Academic Centre for Materials and Nanotechnology, AGH-UST, Krakow, Poland.

See Supplement 1 for supporting content.

REFERENCES

1. K. Ishizaki, M. Koumura, K. Suzuki, K. Gondaira, and S. Noda, "Realization of three-dimensional guiding of photons in photonic crystals," Nat. Photonics **7**, 133–137 (2013).
2. K. Busch, S. Lölkes, R. B. Wehrspohn, and H. Föll, *Photonic Crystals: Advances in Design, Fabrication, and Characterization* (Wiley, 2006).
3. E. Cubukcu, K. Aydin, E. Ozbay, S. Foteinopoulou, and C. M. Soukoulis, "Electromagnetic waves: negative refraction by photonic crystals," Nature **423**, 604–605 (2003).
4. Y. Fang, S.-Y. Leo, Y. Ni, L. Yu, P. Qi, B. Wang, V. Basile, C. Taylor, and P. Jiang, "Optically bistable macroporous photonic crystals enabled by thermoresponsive shape memory polymers," Adv. Opt. Mater. **3**, 1509–1516 (2015).
5. Y. Fang, Y. Ni, S.-Y. Leo, C. Taylor, V. Basile, and P. Jiang, "Reconfigurable photonic crystals enabled by pressure-responsive shape-memory polymers," Nat. Commun. **6**, 7416 (2015).
6. S. John, "Strong localization of photons in certain disordered dielectric superlattices," Phys. Rev. Lett. **58**, 2486–2489 (1987).
7. E. Yablonovitch, "Inhibited spontaneous emission in solid-state physics and electronics," Phys. Rev. Lett. **58**, 2059–2062 (1987).
8. A. Blanco, E. Chomski, S. Grabtchak, M. Ibisate, S. John, S. W. Leonard, C. Lopez, F. Meseguer, H. Miguez, J. P. Mondia, G. A. Ozin, O. Toader, and H. M. van Driel, "Large-scale synthesis of a silicon photonic crystal with a complete three-dimensional bandgap near 1.5 micrometres," Nature **405**, 437–440 (2000).
9. H. Miguez, C. López, F. Meseguer, A. Blanco, L. Vázquez, R. Mayoral, M. Ocana, V. Fornés, and A. Mifsud, "Photonic crystal properties of packed submicrometric SiO2 spheres," Appl. Phys. Lett. **71**, 1148–1150 (1997).
10. C. Becker, S. Linden, G. Von Freymann, M. Wegener, N. Tétreault, E. Vekris, V. Kitaev, and G. Ozin, "Two-color pump-probe experiments on silicon inverse opals," Appl. Phys. Lett. **87**, 091111 (2005).
11. M. Reufer, L. F. Rojas-Ochoa, S. Eiden, J. J. Sáenz, and F. Scheffold, "Transport of light in amorphous photonic materials," Appl. Phys. Lett. **91**, 171904 (2007).
12. K. Edagawa, S. Kanoko, and M. Notomi, "Photonic amorphous diamond structure with a 3D photonic band gap," Phys. Rev. Lett. **100**, 013901 (2008).
13. M. Florescu, S. Torquato, and P. J. Steinhardt, "Designer disordered materials with large, complete photonic band gaps," Proc. Natl. Acad. Sci. USA **106**, 20658–20663 (2009).
14. S. F. Liew, J.-K. Yang, H. Noh, C. F. Schreck, E. R. Dufresne, C. S. O'Hern, and H. Cao, "Photonic band gaps in three-dimensional network structures with short-range order," Phys. Rev. A **84**, 063818 (2011).
15. D. S. Wiersma, "Disordered photonics," Nat. Photonics **7**, 188–196 (2013).
16. N. Muller, J. Haberko, C. Marichy, and F. Scheffold, "Silicon hyperuniform disordered photonic materials with a pronounced gap in the shortwave infrared," Adv. Opt. Mater. **2**, 115–119 (2014).
17. O. Leseur, R. Pierrat, and R. Carminati, "High-density hyperuniform materials can be transparent," Optica **3**, 763–767 (2016).
18. L. S. Froufe-Pérez, M. Engel, P. F. Damasceno, N. Muller, J. Haberko, S. C. Glotzer, and F. Scheffold, "The role of short-range order and hyperuniformity in the formation of band gaps in disordered photonic materials," Phys. Rev. Lett. **117**, 05390 (2016).
19. W. Man, M. Florescu, E. P. Williamson, Y. He, S. R. Hashemizad, B. Y. Leung, D. R. Liner, S. Torquato, P. M. Chaikin, and P. J. Steinhardt, "Isotropic band gaps and freeform waveguides observed in hyperuniform disordered photonic solids," Proc. Natl. Acad. Sci. USA **110**, 15886–15891 (2013).
20. S. A. Rinne, F. García-Santamaría, and P. V. Braun, "Embedded cavities and waveguides in three-dimensional silicon photonic crystals," Nat. Photonics **2**, 52–56 (2008).
21. W. Man, M. Florescu, K. Matsuyama, P. Yadak, G. Nahal, S. Hashemizad, E. Williamson, P. Steinhardt, S. Torquato, and P. Chaikin, "Photonic band gap in isotropic hyperuniform disordered solids with low dielectric contrast," Opt. Express **21**, 19972–19981 (2013).
22. M. Deubel, G. Von Freymann, M. Wegener, S. Pereira, K. Busch, and C. M. Soukoulis, "Direct laser writing of three-dimensional photonic-crystal templates for telecommunications," Nat. Mater. **3**, 444–447 (2004).
23. N. Tétreault, G. von Freymann, M. Deubel, M. Hermatschweiler, F. Perez-Willard, S. John, M. Wegener, and G. A. Ozin, "New route to three-dimensional photonic bandgap materials: silicon double inversion of polymer templates," Adv. Mater. **18**, 457–460 (2006).
24. K. M. Ho, C. Chan, C. Soukoulis, R. Biswas, and M. Sigalas, "Photonic band gaps in three dimensions: new layer-by-layer periodic structures," Solid State Commun. **89**, 413–416 (1994).
25. M. Hermatschweiler, A. Ledermann, G. A. Ozin, M. Wegener, and G. von Freymann, "Fabrication of silicon inverse woodpile photonic crystals," Adv. Mater. **17**, 2273–2277 (2007).
26. I. Staude, M. Thiel, S. Essig, C. Wolff, K. Busch, G. Von Freymann, and M. Wegener, "Fabrication and characterization of silicon woodpile photonic crystals with a complete bandgap at telecom wavelengths," Opt. Lett. **35**, 1094–1096 (2010).

27. A. Frölich, J. Fischer, T. Zebrowski, K. Busch, and M. Wegener, "Titania woodpiles with complete three-dimensional photonic bandgaps in the visible," Adv. Mater. **25**, 3588–3592 (2013).
28. J. Haberko and F. Scheffold, "Fabrication of mesoscale polymeric templates for three-dimensional disordered photonic materials," Opt. Express **21**, 1057–1065 (2013).
29. J. Haberko, N. Muller, and F. Scheffold, "Direct laser writing of three-dimensional network structures as templates for disordered photonic materials," Phys. Rev. A **88**, 043822 (2013).
30. C. Song, P. Wang, and H. A. Makse, "A phase diagram for jammed matter," Nature **453**, 629–632 (2008).
31. D. Chandler-Horowitz and P. M. Amirtharaj, "High-accuracy, midinfrared (450 $cm^{-1} \leq \omega \leq$ 4000 cm^{-1}) refractive index values of silicon," J. Appl. Phys. **97**, 123526 (2005).
32. A. F. Oskooi, D. Roundy, M. Ibanescu, P. Bermel, J. D. Joannopoulos, and S. G. Johnson, "MEEP: a flexible free-software package for electromagnetic simulations by the FDTD method," Comput. Phys. Commun. **181**, 687–702 (2010).
33. C. Marichy, N. Muller, L. S. Froufe-Pérez, and F. Scheffold, "High-quality photonic crystals with a nearly complete band gap obtained by direct inversion of woodpile templates with titanium dioxide," Sci. Rep. **6**, 21818 (2016).
34. G. Von Freymann, A. Ledermann, M. Thiel, I. Staude, S. Essig, K. Busch, and M. Wegener, "Three-dimensional nanostructures for photonics," Adv. Funct. Mater. **20**, 1038–1052 (2010).
35. P. Mueller, M. Thiel, and M. Wegener, "3D direct laser writing using a 405 nm diode laser," Opt. Lett. **39**, 6847–6850 (2014).